Theor Chim Acta (1989) 75: 333-352

Theoretica Chimica Acta

Discrete characterization of cross-sections of molecular surfaces

Gustavo A. Arteca and Paul G. Mezey

Department of Chemistry and Department of Mathematics, University of Saskatchewan, Saskatoon, Saskatchewan, S7N 0W0 Canada

(Received June 1, revised September 6/Accepted September 12, 1988)

The three-dimensional shape of molecules can be described by appropriately chosen, formal molecular surfaces, such as electronic isodensity contours, molecular electrostatic isopotential contours, and similar functions. The characterization of the shape of such molecular surfaces, in particular, their changes along reaction paths, is of importance in several areas of theoretical and applied chemistry, biochemistry, and pharmacology. Molecular shapes are often represented in terms of *cross-sections* of such molecular surfaces, by appropriately chosen planes. Thus, the characterization of 3D shape is transformed into the 2D problem of characterizing a number of plane curves, the cross-sections. The problem is further simplified if these *continuous* curves are characterized using the methods of *discrete* mathematics, which are often more suitable for computer applications. In this work we formalize a number of possible approaches to provide a discrete characterization of molecular surface cross-sections. The method is graph-theoretical in nature and it allows one to provide a concise description of the curves, and their changes with the rearrangements in the nuclear configuration. The vertices of the graph are the inflexion points of the cross-section and the edges are their mutual visibility relations. The procedure is easily programmable as an algorithm, permitting an automatic evaluation of the shape descriptors for a large number of cross-sections and molecules. This possibility is of importance with respect to molecular similarity studies of computer-assisted drug design. Several simple examples are chosen to illustrate the shape descriptors. The basic ideas are illustrated by detailed cross-sections of the electronic density for the

molecule of water, as functions of changes in bond angle and bond lengths. Molecular electrostatic maps for molecules of biochemical interest (nucleotide bases) are analyzed with respect to shape similarities. Finally, some of the notions are generalized to deal with cross-sections of surfaces of hard-sphere molecular models (the so-called van der Waals surfaces).

Key words: Characterization of molecular shape — Molecular similarity — Computer-assisted drug design — Topology and graph theory

1. Introduction

The shape of a molecule is recognized to play an important role in determining some of its characteristic physical and chemical properties. The study of molecular shape is of considerable interdisciplinary interest: shape characterization of molecules has become essential in computer-assisted drug design [1-3].

The concept of molecular shape is very different from the shape concept of macroscopic solid bodies, due to the fact that there exists no rigorously defined geometrical surface that encloses the entire molecule. At the peripheral regions of a molecule one finds a fuzzy electronic charge cloud, and even the nuclear positions are not precisely defined due to vibrational motion, and on a more fundamental level, due to quantum-mechanical uncertainty. Nevertheless, several, appropriately defined, formal molecule surfaces have been found to provide useful descriptors for certain physical properties. This constitutes a pragmatic approach, where one may define and characterize a different molecular surface depending on the property one is interested in. Constant molecular electrostatic potential contours [4-17], electronic isodensity surfaces [18-20], surfaces of hard-sphere molecular models (the so-called van der Waals surfaces [VDWSs]) [21-23], or superimposed surfaces representing interrelations of any two of the above surfaces [24], are among the possible choices.

A full characterization of molecular surfaces is a continuum problem in 3-space. Several approaches have been proposed recently in the literature. Correlation coefficients for pairs of electron density functions [25-29] have been used to quantify similarity in pairs of molecules. In the case of VDWSs, a partial shape characterization can be given in terms of the solvent accessibility regions of the hard-sphere surface [23, 30-32], or in terms of the surface's fractal dimension [33-35]. A recent approach, converting the continuum problem of the shape of three-dimensional molecular surfaces into a discrete problem, is the so-called "shape group method" (SGM) [36-45]. This method is based on the representation of the common *geometrical* features of a family (a continuum) of possible geometrical contour surfaces by a *topological* object, and on the computation of a number of topological invariants, the incidence relations and shape groups [26-29]. These shape groups are the homology groups of a hierarchy of truncated surfaces related to the molecular surfaces. The method has been used to study both isodensity and isopotential contours [36-39], as well as the influence of conformational changes on their shape [39, 40], van der Waals surfaces [40-43], and the mutual interpenetration of pairs of molecular surfaces [44, 45]. Some

comments on the description of shapes of molecular orbital surfaces can be found in [46].

Despite the recent developments in the study of molecular surfaces, a great part of the analysis currently reported in the literature is performed on *cross-sections* of surfaces. The three-dimensional entity is replaced by a number of (in principle, infinitely many) plane curves. As far as we know, no attempt has been made up till now to provide a concise and nonvisual (algorithmic) description of the cross-sections of molecular surfaces, by means comparable to the SGM employed with the surfaces themselves. The purpose of this note is to fill this gap.

The basic idea is the assignment of a graph [47] to every plane curve. Graph-theoretical approaches to the description of *molecular surfaces* have recently been introduced in the literature [48–50]. These graphs are associated to a three-dimensional entity, such as the entire "body" of the molecular electron distribution, and they bear no relationship with the usual molecular graphs built from atoms and bonds within a molecule [See Refs. quoted in [48–50]]. The molecular surface graphs provide a simple, pictorial, yet nontrivial, representation of both differentiable [48] and non-differentiable [49] surfaces, whereas seeing graphs of closed contour surfaces [50] are applicable to both types of problems. In this work we follow a conceptually similar approach to describing the cross-sections of a molecular surface, where we take advantage of the special features of the 2D problem.

The graph we propose in this study for each cross-section curve can be characterized by matrices, that contain the information on distances and visibility of selected points [50] as well as other specific properties from the curve. This approach provides a *discrete* description of the molecular surface cross-sections that can be easily stored and retrieved from a computer. By this procedure, essential information about the surface is represented by a number of matrices, providing an algorithmic tool for the shape comparison of different molecules. There exists another aspect worth mentioning. As it is known, the essential shape features of the cross-sections do not always change with the changes in nuclear conformations (see discussions in [39, 40]). Accordingly, the graph-theoretical characterization of the planar curves provides a tool for the analysis of the role of the configurational rearrangements in inducing essential changes in shape.

In this note a family of cross-section graphs of the molecular surface is defined and constructed. Several illustrative applications are provided, using contours of electronic density and molecular electrostatic potentials. The extension to define similar graphs for the VDWSs is also briefly discussed.

2. Graphs for cross-sections of molecular surfaces

Consider a closed contour surface in 3-space ${}^3\mathbb{R}$, not necessarily homeomorphic to a 2-sphere, obtained as a boundary of a level set F of a given molecular function $f(\boldsymbol{r})$, such as electronic charge density, where $\boldsymbol{r} \in {}^3\mathbb{R}$. This contour surface

will be represented as $G(a, K)$. The level set and its boundary are given by

$$F(a, K) = \{\boldsymbol{r} \in {}^3\mathbb{R}: f(\boldsymbol{r}) \geq a\}, \tag{1a}$$

$$G(a, K) = \{\boldsymbol{r} \in {}^3\mathbb{R}: f(\boldsymbol{r}) = a\}, \tag{1b}$$

where K is an element of the reduced nuclear configuration space M, $K \in M$ [51]; K represesents an internal nuclear configuration. Note that the level set $F(a, K)$ is bounded, if the high function values are found near the nuclei. Let P be a plane in 3-space:

$$P = P(A_1, A_2, A_3, A_4) = \{\boldsymbol{r} \in {}^3\mathbb{R}: A_1 x + A_2 y + A_3 z = A_4\}, \qquad \boldsymbol{r} = (x, y, z). \tag{2}$$

A cross-section c of the surface G is then given as follows:

$$c = G(a, K) \cap P(A_1, A_2, A_3, A_4). \tag{3}$$

If the intersection (3) is not empty, then the set c will consist of a number of closed planar curves, satisfying an equation of the form $\phi_c(\boldsymbol{r}) = 0$. The occurrence of a single point $\boldsymbol{p}$ as a cross-section, when P is a plane tangent to the surface G, can be seen as a degenerate closed curve.

We shall characterize the curve $\phi_c(\boldsymbol{r}) = 0$ by means of a graph, that will be denoted by $g_n(a, K, P)$, where n stands for its number of vertices.

Let u and v be a pair of orthogonal axes spanning the generic plane P. Any point $\boldsymbol{p}$ in P can be represented by a pair (u, v). The location of this point $\boldsymbol{p}$ in 3-space in terms of the triplet (x, y, z) can be determined knowing the equation of the plane. The cross-section is representable in plane P as a multi-valued function $v = h(u)$. For any generic point $\boldsymbol{p}_i(P)$ belonging to the curve, $\boldsymbol{p}_i(P) = (u_i, v_i) \in P \subset {}^3\mathbb{R}$, $v_i = h(u_i)$. Furthermore, by analogy with the $(3N-6)$-dimensional case of curvature analysis of reactive domains of potential surfaces [51, 52] one can define for every point on the curve a local, orthogonal system of coordinates in terms of the tangent $\boldsymbol{U}$ and normal vector $\boldsymbol{V}$ to the curve at the point. The orientation of $\boldsymbol{V}$ is taken as that of the negative gradient of function $f_P(\boldsymbol{r})$ at point $\boldsymbol{p}$, if the level set $F(a, K)$ is bounded, and as that of the gradient otherwise, where $f_P(\boldsymbol{r})$ is the restriction of function $f(\boldsymbol{r})$ to plane P. The choice between the two possible orientations of $\boldsymbol{U}$ has no significance concerning the final formulas of the method proposed in this study.

This system of axes is indicated as (U, V) [See Fig. 1 for an explanation]. The transformation between the two systems is obtained simply by rotation and translation:

$$U = (u - u_i) \cos \theta_i + (v - v_i) \sin \theta_i, \tag{4a}$$

$$V = -(u - u_i) \sin \theta_i + (v - v_i) \cos \theta_i, \tag{4b}$$

where the angle θ_i is given by

$$\theta_i = \arctan \{h'_u(u_i)\}, \qquad h'_u(u_i) = (dh/du)_{(u=u_i)}. \tag{5}$$

In the new system of coordinates the function representing the cross-section is written as $V = H(U)$. We use the notation $h'_u, h''_u, \ldots$ when referring to the derivatives in the coordinate frame for plane P, and $H'_U, H''_U, \ldots$ is used for the

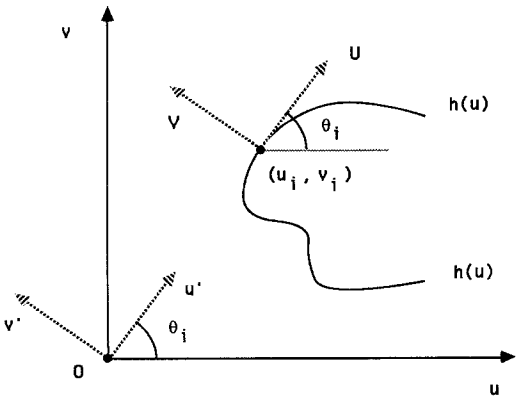

Fig. 1. Definition of a local system of coordinates for every point belonging to the molecular surface cross-section. The drawing represents a generic plane $P(A_1, A_2, A_3, A_4)$

derivatives in the local system of coordinates at the generic point $\boldsymbol{p}_i$. The construction and characterization of the graph involve some of these derivatives. A simple computation with Eqs. (4) leads to the following relations:

$$H'_U = [h'_u \cos\theta_i - \sin\theta_i]/[h'_u \sin\theta_i + \cos\theta_i], \tag{6}$$

$$H''_U = h''_u/(h'_u \sin\theta_i + \cos\theta_i)^3, \tag{7}$$

$$H'''_U = [h'''_u(h'_u \sin\theta_i + \cos\theta_i) - 3(h''_u)^2 \sin\theta_i]/(h'_u \sin\theta_i + \cos\theta_i)^5. \tag{8}$$

At the point $\boldsymbol{p}_i$ (origin of the local system of coordinates) we have $U = 0$. If $h'_u(u = u_i)$ is finite one finds at this point:

$$H'_U(0) = 0, \tag{9a}$$

$$H''_U(0) = \cos^3\theta_i \, h''_u(u_i), \tag{9b}$$

Eq. (9a) follows from the very definition of the local system of coordinates (that is, every point $\boldsymbol{p}_i$ is a critical point in its own local frame). Equation (9b) shows that the inflexion points in the coordinate frame of P will remain inflexion points within the local system. In this particular case, i.e. when $\boldsymbol{p}_i$ is an inflexion point, we find:

$$H'''_U(0) = \cos^4\theta_i \, h'''_u(u_i). \tag{9c}$$

When $1/h'_u(u_i) = 0$, then the treatment is slightly different, but the same conclusion remains valid for the inflexion points. In this latter case one should notice that h and H are related as follows:

$$H(U) = u_i - h^{-1}(U + u_i), \tag{10}$$

where $h^{-1}(u)$ represents the inverse function.

In the following we shall assume that c does not contain straight line segments. The vertices of the graph $g_n(a, K, P)$, collected in the set $V(g_n)$, are the local inflexion points of the cross-section c:

$$\begin{aligned} V(g_n(a, K, P)) &= \{\boldsymbol{p}_i \in P \subset {}^3\mathbb{R}\colon H''(\boldsymbol{p}_i) = 0\} \\ &= \{\boldsymbol{V}_1, \boldsymbol{V}_2, \ldots, \boldsymbol{V}_n\}, \end{aligned} \tag{11}$$

where $H''(\boldsymbol{p}_i)$ stands for the second derivative within the local system at point $\boldsymbol{p}_i$. It is evident that if the curve is closed, n will be either zero or an even positive number. The case $n=0$ (i.e., no graph) corresponds to a convex curve $\phi_c(\boldsymbol{r})=0$.

These vertices divide the cross-section into domains of different concavity. A section of the curve between the points $\boldsymbol{V}_j$ and $\boldsymbol{V}_{j+1}$ is concave if $H''>0$ at the local system of every point of the section. On the other hand, if $H''<0$ then the section will be convex.

The ordering given to the vertices of the graph is arbitrary. In this work we use the following convention: The n vertices are numbered in order of occurrence when moving along the curve, so that the section between $\boldsymbol{V}_1$ and $\boldsymbol{V}_2$ is concave.

In order to complete the construction of the graph we need to define its edges. This can be done by a number of possible neighbor relations among vertices. In this work we use the condition of "visibility between vertices", because it allows one to describe some shape features of the cross-section (in this case, an indication of the extent of its indentations). This visibility relation is defined as follows. Let c^* be the union of c and the bounded subset of P it encloses, that is,

$$c^* = F(a, K) \cap P(A_1, A_2, A_3, A_4), \tag{12a}$$

if the level set $F(a, K)$ is bounded, and

$$c^* = \text{clos}\{F^c(a, K)\} \cap P(A_1, A_2, A_3, A_4), \tag{12b}$$

otherwise, where $\text{clos}\{F^c(a, K)\}$ is the closure of the complement $F^c(a, K)$ of $F(a, K)$.

Two vertices $\boldsymbol{V}_i$ and $\boldsymbol{V}_j$ (points in 3-space) are *visible* to each other if the straight line segment joining them is totally contained in c^*. Formally, this is described by the relation "vis" given as:

$$\text{vis}(\boldsymbol{V}_i, \boldsymbol{V}_j) = \begin{cases} 1, & \text{if: } \boldsymbol{V} = \alpha \boldsymbol{V}_i + (1-\alpha)\boldsymbol{V}_j \in c^*, \ \forall \alpha \in [0, 1] \\ 0, & \text{otherwise.} \end{cases} \tag{13}$$

The relation of visibility is comparable to the one used in [50] to define the so-called "seeing graphs".

The edges of the graph, collected in the set $E(g_n(a, K, P))$, are given by the pairs $(\boldsymbol{V}_i, \boldsymbol{V}_j)$ satisfying the relation of visibility:

$$E(g_n(a, K, P)) = \{(\boldsymbol{V}_i, \boldsymbol{V}_j): \text{vis}((\boldsymbol{V}_i, \boldsymbol{V}_j)) = 1\}. \tag{14}$$

The graphs defined by Eqs. (11) and (14) will be termed a *visibility graph for the inflexion points of the cross-section c.* This graph can be characterized in several possible ways, for example, in terms of its *visibility matrix*, given as:

$$\boldsymbol{v}(g_n) = (\boldsymbol{v}_{ij}); \qquad \boldsymbol{v}_{ij} = \text{vis}((\boldsymbol{V}_i, \boldsymbol{V}_j)). \tag{15}$$

The matrix $\boldsymbol{v}(g_n)$ is symmetric and its diagonal elements are unity. In fact, the visibility matrix is the sum of the n-dimensional unit matrix and the adjacency matrix of the visibility graph $g_n(a, K, P)$. Using the convention for the numbering

of vertices, if c is a single Jordan curve, one obtains for the off-diagonal elements one position removed from the diagonal:

$$v_{i,i+1} = 0, \qquad v_{i+1,i+2} = 1, \qquad i = 1, 3, 5, \ldots . \tag{16}$$

Notice, however, that property (16) does not necessarily hold if the cross-section is formed by *several* closed curves.

The case of a convex curve is special, since no inflexion point occurs on the cross-section. Nevertheless, the characterization can be formally extended to this case. We assign the matrix $v = [0]$ as a formal visibility matrix to each convex cross-section. As a comparison, notice that if a curve possesses a single inflexion point (the curve must extend to infinity) it will be represented by a visibility matrix $v = [1]$ (an inflexion point always sees itself).

Changes in the level set parameter a, in the nuclear configuration K, or a different choice of an intersection plane P, will lead to variations in the shape of the cross-section c and its associated graph $g_n(a, K, P)$. These differences may correspond to the occurrence of disappearance of vertices (changes in n), as well as to changes of their visibility (changes in the matrix elements v_{ij}). Changes in the visibility matrix reveal changes in the extent of the concave indentations and convex protuberances.

As an illustrative example of above ideas consider the case depicted in Fig. 2. The closed curve c represents a cross-section for a function $f(\boldsymbol{r})$. It is understood that in this case $F(a, K)$ is bounded, and one finds the high function values within c^*. The visibility is given in terms of straight line segments lying within c^*. The right half of the figure displays the result obtained for the graph. One notices, for example, the alternation in visibility of consecutive points (i.e., V_1 does not see V_2, V_2 does see V_3, and so forth). As the graph shows, the vertices

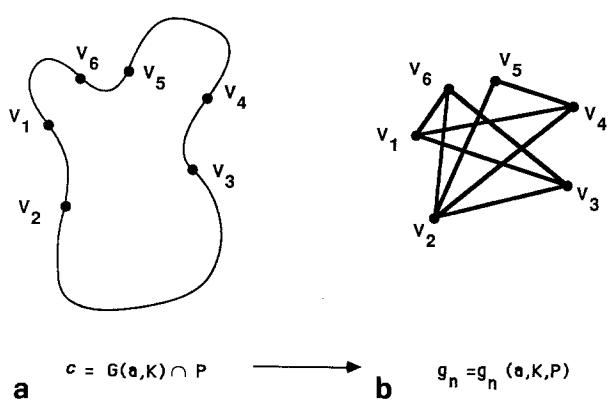

Fig. 2a, b. Example of construction of the visibility graph from a planar, *closed curve*, representing a cross-section of some generic molecular surface. **a** Cross-section; **b** visibility graph of inflexion points

labelled 1, 3, 4, and 6 each see three other vertices, whereas the vertex 2 sees four and vertex 5 only two vertices besides themselves.

One can obtain a complementary characterization of the cross-sections in terms of the distances between vertices. This adds information related to the size of the molecular surface, not necessarily taken into account by the visibility matrix. One may combine both sets of information in the matrix $\boldsymbol{D}(g_n)$:

$$\boldsymbol{D}(g_n) = [(\boldsymbol{D}(g_n))_{ij}], \qquad (\boldsymbol{D}(g_n))_{ij} = \boldsymbol{v}_{ij} \| \boldsymbol{V}_i - \boldsymbol{V}_j \| . \tag{17}$$

This matrix has as elements the distances between vertices that *see each other*, and zeroes for vertex points that do not.

There are many other possible variants of the above method that may be useful in shape analysis. The matrix of third derivatives at the local inflexion points (cf. Eq. (9c)) provides some additional information not present in the previous two matrices. The length of concave and convex segments along the cross-sections usually correlate with the extreme values of the local second derivative for points lying between two consecutive vertices. These points with extreme values of second derivatives could be taken as the vertices of an alternative visibility graph description of the cross-section. By reversing the orientation of vector $\boldsymbol{V}$, one obtains the *exterior visibility graph* of c.

In the next section we confine ourselves to the simplest description of molecular surface cross-section by using the visibility matrix $\boldsymbol{v}$.

3. Applications of the method: electronic density and nuclear rearrangements

As a first illustrative example we consider the graph-theoretical description of changes in shapes in molecular surface cross-sections induced by conformational rearrangements.

The examples chosen are cross-sections of the total electronic density of the molecule of water, across the molecular plane defined by the fixed nuclear positions. The total density was computed for every nuclear geometry at *ab initio* level using the program HONDO-7.0 of Dupuis and co-workers [53], with a DZP basis set, in particular, Dunning's $(9s, 5p)/[3s, 2p]$ with polarization functions on both O and H. With this basis set the equilibrium OH bond length and HOH bond angle α are 0.944 Å and 106.5°, respectively. In order to cover the most important differences in shape, the following cross-sections of the electronic density have been computed: $a = 0.2$, 0.02, 0.002, and 0.001 e/bohr^3.

Two types of geometry changes have been studied for the above contours. The first is the bending motion that conserves the C_{2v} symmetry. In this case, the OH distances were kept at their equilibrium value, and the bond angle α was varied from 5° to 180°. At $\alpha = 180°$ the symmetry becomes $D_{\infty h}$.

The three outermost contours ($a = 0.02$, 0.002, and 0.001 e/bohr^3) shows a similar change in shape as described by the visibility matrices $\boldsymbol{v}(a, \alpha)$ of the cross-section

graphs. Four different matrices v_s, $s = 1, 2, 3, 4$, occur when changing the bond angle α:

$$v_1 = \begin{bmatrix} 1 & 0 & 1 & 1 \\ 0 & 1 & 1 & 1 \\ 1 & 1 & 1 & 0 \\ 1 & 1 & 0 & 1 \end{bmatrix} \rightarrow v_2 = [0] \rightarrow v_3 = \begin{bmatrix} 10 \\ 01 \end{bmatrix} \rightarrow v_4 = [0]. \tag{18}$$

The matrices v_s are found for different angles for the various cross-sections:

$v(0.02, 5°) = v(0.002, 5°) = v(0.001, 5°) = v_1$;
$v(0.02, 35°) = v(0.002, 35°) = v(0.001, 35°) = v_2$;
$v(0.02, 65°) = v(0.002, 65°) = v(0.001, 65°) = v_3$;
$v(0.02, 105°) = v(0.002, 125°) = v(0.001, 145°) = v_4$.

Notice that the first appearance of matrix $v_4(\alpha)$ $(= v_2(\alpha))$, occurs at different values of α for different contours. This difference is easily understood. Both v_4 and v_2 represent convex curves, and the outermost cross-sections become convex curves when the two hydrogen atoms are far enough from each other. If the contour is further away from the nuclei, then a smaller bond angle is needed to make the cross-section convex.

The innermost cross-section ($a = 0.2$) reveals a much richer structure when the bond angle changes. Figure 3 shows a superposition of these cross-sections of the electronic density surface. This figure allows one to appreciate the role of the conformational rearrangements in reshaping the cross-section curve. In this case a larger number of inflexion points are found during the transformation. For very small angles the two hydrogen atoms almost collapse, an unlikely situation which is represented by a curve with two concave and two convex sections (four inflexion points). On the other hand, for angles close to 180° one finds an arrangement with four convex and four concave regions (eight inflexion points). The overall situation is described in Fig. 4, which shows the various visibility matrices found during the scanning of bond angles. The approximate bond angle value at which a given graph occurs is given in parentheses.

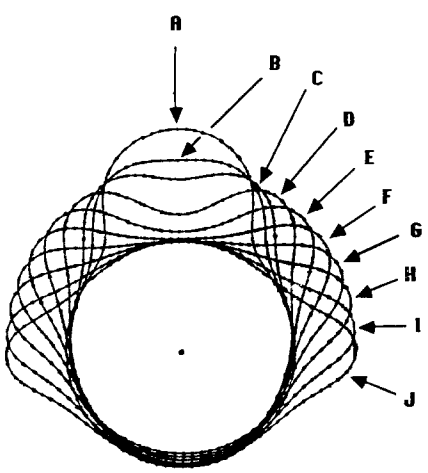

Fig. 3. Superimposed cross-sections of the electronic density contour $a = 0.2$ e/bohr^3 of water along a bending vibration with symmetry C_{2v}. The curves lie on the molecular plane; the oxygen atom is at the origin. *A*: 25°; *B*: 35°; *C*: 45°; *D*: 65°; *E*: 85°; *F*: 105°; *G*: 125°; *H*: 145°; *I*: 165°; *J*: 180°

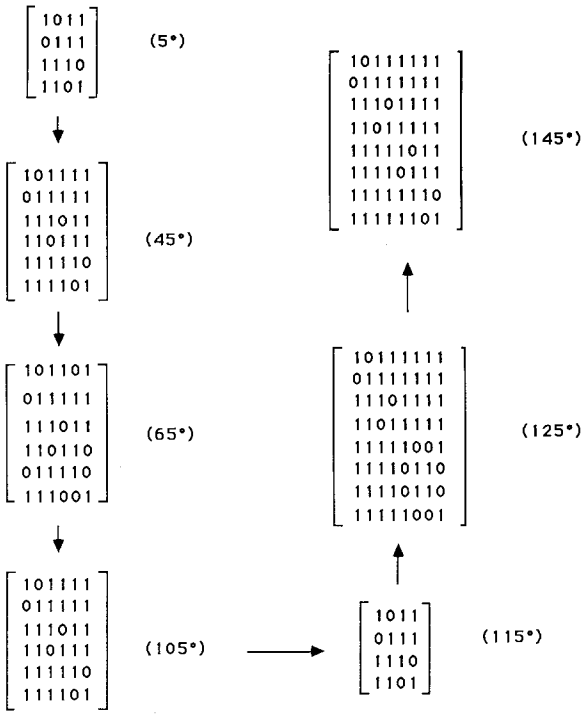

Fig. 4. Visibility matrices for the graphs of the electronic density cross-section of water at $a = 0.2$ e/bohr^3, corresponding to the bending with symmetry C_{2v}

Another interesting feature shown in Fig. 3 is the occurrence of an approximately circular region about the oxygen atom, which is not entered by the contour lines. This region seems to be almost completely unaffected by the conformational motion of the two hydrogen atoms, and so it constitutes a property characteristic of the oxygen atom. This property provides a very attractive basis to construct a scale of van der Waals radii from first principles [54].

Bendings of an asymmetrically stretched molecule, leading from symmetry C_s to $C_{\infty v}$ as α increases, have been compared with the previous results. In this case, the same scanning of bond angles was performed, but one of the OH bonds was stretched up to 1.40 Å. The second bond length was kept at its equilibrium value. The results for the visibility matrices of various cross-sections considered are shown in Fig. 5.

A most interesting case is the set of contours for the value $a = 0.2$ e/bohr^3. Similarly to the case of symmetry C_{2v} shown in Fig. 3, Fig. 6 displays a superimposed view of the corresponding curves. The outstanding feature is the occurrence of a critical angle for which the single closed curve breaks up into two closed curves. One of these curves is always convex, that shrinks as α increases, and finally disappears when the two hydrogen atoms are far enough from each other (corresponding to a bond angle slightly larger than 135°). The occurrence of the

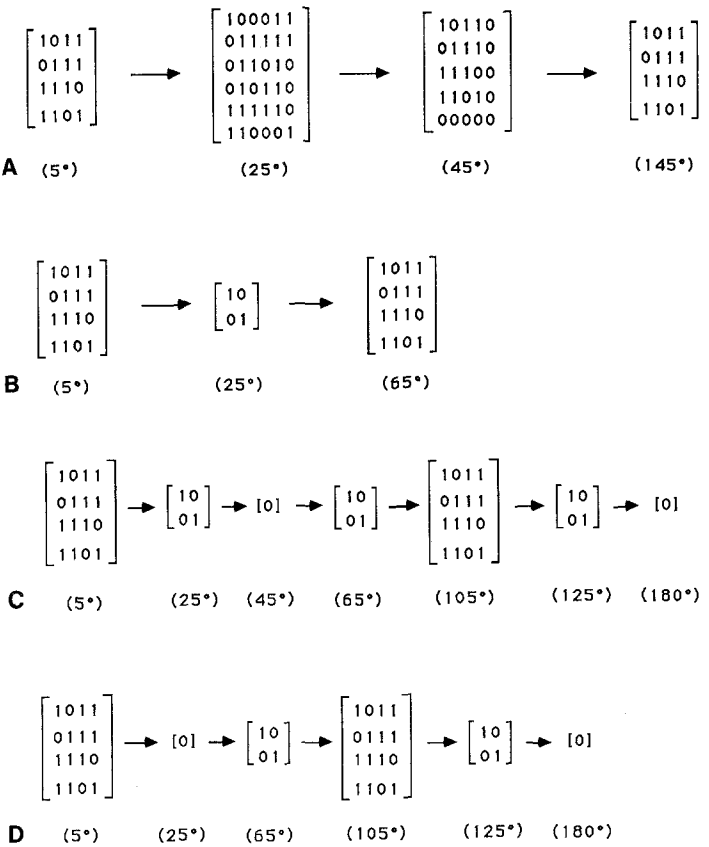

Fig. 5. Visibility matrices for the graphs of a number of electronic density cross-sections of water corresponding to a bending with symmetry C_s. The labels *A*, *B*, *C* and *D* stand for the level set constants $a = 0.2$, 0.02, 0.002 and 0.001 e/bohr^3, respectively

two curves forming a cross-section is reflected in the visibility graph and its visibility matrix. The third matrix in the first line of Fig. 5 has a fifth row and a fifth column both containing only zeroes, corresponding to the separate, convex curve. Notice that the curve that does not disappear remains approximately constant during the motion of the hydrogen atom. These approximately coincident curves define a region of space that encloses an OH group, whose properties are mostly unaffected by the presence of the other atom. As mentioned earlier, this property has some promising consequences with regard to the determination of atomic van der Waals radii or transferable properties associated with chemical groups [54].

The examples shown in this section illustrate the application of the proposed method. It is noteworthy that the visibility properties of the graph allow one to recognize the occurrence of many of the essential changes in shape due to the

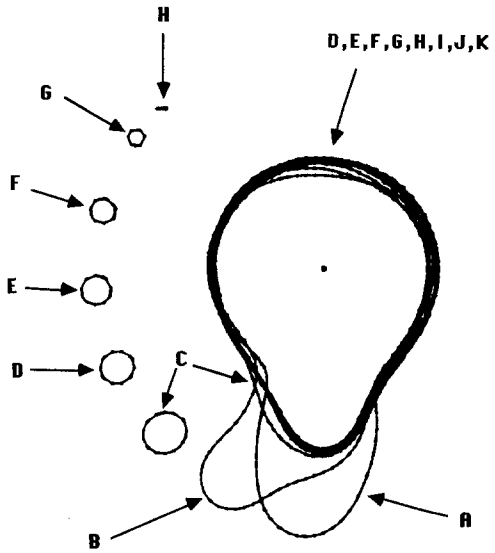

Fig. 6. Superimposed cross-sections of the electronic density contour $a = 0.2$ e/bohr^3 of water along a bending vibration with symmetry C_s. The curves lie on the molecular plane; the oxygen atom is at the origin. Notice that on the right-hand side of the figure the contours labelled *D, E, F, G, H, I, J* and *K* are hardly distinguishable from one another. Bond angles, *A*: 5°; *B*: 25°; *C*: 45°; *D*: 65°; *E*: 85°; *F*: 105°; *G*: 125°; *H*: 135; *I*: 145°; *J*: 165°; *K*: 180°

conformational rearrangements. This approach may be also of interest to provide a discrete characterizatioon of shape transformations in molecular surfaces undergoing chemical reactions. In this latter case the choice of the planes to obtain the cross-sections can be decided based on the directions in which two or more reagents approach one another.

4. Further applications: molecular electrostatic potential maps

Molecular electrostatic potential (MEP) maps provide a molecular surface frequently used for the interpretation of biochemical activity [4–17]. The shape of these MEP surfaces (or the shape features of their relevant cross-sections) are of particular interest to rationalize similarities between compounds and to detect the number and type of reactive centers of a molecule [4–17, 55]. In this section we provide a brief, illustrative analysis of the shape of these maps in terms of the formalism proposed above.

As an example, we have considered the analysis of the MEP cross-sections for a family of compounds of major interest: the DNA pyrimidine and purine basis, namely cytosine, uracil, adenine, and guanine. The MEP's of these compounds have been obtained from the literature, and need not be recomputed here. In our case we have made use of the recent results computed by Eisenstein [56]; the MEP's are constructed from *ab initio* 4-31G atomic multipoles. The cross-sections studied are those within the plane containing the ring nuclei of the molecules. All the four compounds mentioned above present both positive (proton repelling) and negative (proton attracting) regions of potential. The cross-sections for all these regions of MEP appear as one or more closed planar curves. The zero contour, on the other hand, always contains at least one open curve, extending

to infinity. The cross-section visibility graphs can be built easily providing a discrete characterization for these MEP maps.

Figure 7 shows schematically some typical cross-sections for cytosine. This provides an illustration of the overall pattern found or all the compounds, and it is not intended to be complete or accurate. For cytosine, Table 1 provides a complete characterization of the cross-section in terms of the visibility matrices obtained from the results in [56]. For the contours with zero or negative MEP we quote the *exterior visibility* (reversing $V \to -V$ in the local frame; cf. Sect. 2). Table 1 shows that the curves' features become more complicated when the MEP level set value a increases. This is a reasonable result, since for larger values of positive MEP the convex sections of the contour follow closely the position of the atoms. Accordingly, these cross-sections exhibit a different number and different visibility interrelations of inflexion points, when compared to the looser and more featureless cross-sections.

Table 2 displays the results for the visibility matrices of the MEP contours corresponding to a values of +4 and −4 kcal/mol, for cytosine, uracil, adenine, and guanine. The results in the table are easily interpreted. Let us consider, for example, the negative MEP contours (analyzed according to the exterior visibility graphs). For cytosine we find a 4×4 matrix with zeroes and ones, but with no rows or columns having only zeroes. This corresponds to a cross-section which is a single closed curve. For uracil and adenine we find visibility matrices involving only elements equal to one. This corresponds to the visibility of a number of closed curves, each one invoking inflexion points mutually visible. This can only take place if each curve contains two inflexion points and the contour function (MEP here) is such that $F(a, K)$ is unbounded. One concludes then that uracil must possess two of such closed curves and adenine three of them. The interior of any of such closed curves encloses one minimum of the electrostatic potential. Finally, guanine shows a column and a row of zeroes. This clearly indicates that

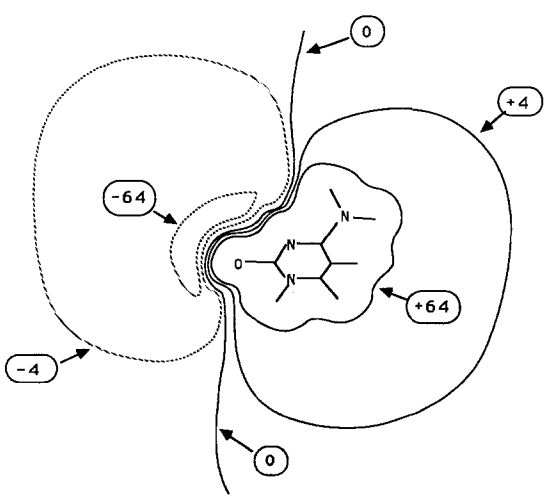

Fig. 7. Schematic representation of cross-sections of MEP for cytosine along the molecular plane. The values indicated in the figure are in kcal/mol

Table 1. Visibility matrices for several cross-sections of the molecular electrostatic potential of cytosine (planar configuration). The exterior visibility graph is used for the zero and negative MEP contours

MEP level set value (kcal/mol)	Visibility matrix
−64	$\begin{bmatrix} 1 & 1 \\ 1 & 1 \end{bmatrix}$
−32, −16, −8, −4	$\begin{bmatrix} 1 & 1 & 1 & 1 \\ 1 & 1 & 0 & 0 \\ 1 & 0 & 1 & 1 \\ 1 & 0 & 1 & 1 \end{bmatrix}$
0	$\begin{bmatrix} 1 & 0 & 0 & 0 & 0 & 0 \\ 0 & 1 & 1 & 0 & 1 & 0 \\ 0 & 1 & 1 & 0 & 1 & 0 \\ 0 & 0 & 0 & 1 & 1 & 0 \\ 0 & 1 & 1 & 1 & 1 & 0 \\ 0 & 0 & 0 & 0 & 0 & 1 \end{bmatrix}$
+4, +8, +16	$\begin{bmatrix} 1 & 0 & 0 & 0 & 0 & 0 \\ 0 & 1 & 1 & 0 & 1 & 1 \\ 0 & 1 & 1 & 0 & 1 & 0 \\ 0 & 0 & 0 & 1 & 1 & 0 \\ 0 & 1 & 1 & 1 & 1 & 0 \\ 0 & 1 & 0 & 0 & 0 & 1 \end{bmatrix}$
+32	$\begin{bmatrix} 1 & 0 & 1 & 0 & 1 & 0 & 1 & 1 & 1 & 1 & 1 & 1 & 1 & 1 \\ 0 & 1 & 1 & 0 & 0 & 0 & 1 & 1 & 1 & 1 & 1 & 1 & 1 & 1 \\ 1 & 1 & 1 & 0 & 0 & 0 & 0 & 0 & 0 & 1 & 1 & 1 & 1 & 1 \\ 0 & 0 & 0 & 1 & 0 & 0 & 1 & 1 & 1 & 1 & 1 & 1 & 1 & 1 \\ 1 & 0 & 0 & 0 & 1 & 0 & 1 & 0 & 1 & 1 & 1 & 1 & 1 & 1 \\ 0 & 0 & 0 & 0 & 0 & 1 & 1 & 0 & 1 & 1 & 1 & 1 & 1 & 1 \\ 1 & 1 & 0 & 1 & 1 & 1 & 1 & 0 & 0 & 0 & 1 & 1 & 1 & 1 \\ 1 & 1 & 0 & 1 & 0 & 0 & 0 & 1 & 1 & 0 & 1 & 1 & 1 & 1 \\ 1 & 1 & 0 & 1 & 1 & 1 & 0 & 1 & 1 & 0 & 0 & 1 & 1 & 1 \\ 1 & 1 & 1 & 1 & 1 & 1 & 0 & 1 & 0 & 1 & 1 & 0 & 1 & 1 \\ 1 & 1 & 1 & 1 & 1 & 1 & 1 & 1 & 1 & 1 & 1 & 0 & 0 & 0 \\ 1 & 1 & 1 & 1 & 1 & 1 & 1 & 1 & 1 & 0 & 0 & 1 & 1 & 0 \\ 1 & 1 & 1 & 1 & 1 & 1 & 1 & 1 & 1 & 1 & 0 & 1 & 1 & 0 \\ 1 & 1 & 1 & 1 & 1 & 1 & 1 & 1 & 1 & 1 & 0 & 0 & 0 & 1 \end{bmatrix}$
+64	$\begin{bmatrix} 1 & 0 & 1 & 0 & 1 & 0 & 1 & 1 & 1 & 1 & 1 & 1 & 1 & 1 \\ 0 & 1 & 1 & 0 & 0 & 0 & 1 & 1 & 1 & 1 & 1 & 1 & 1 & 1 \\ 1 & 1 & 1 & 0 & 0 & 0 & 0 & 0 & 0 & 1 & 1 & 1 & 1 & 1 \\ 0 & 0 & 0 & 1 & 0 & 0 & 1 & 1 & 1 & 1 & 1 & 1 & 1 & 1 \\ 1 & 0 & 0 & 0 & 1 & 0 & 1 & 0 & 1 & 1 & 1 & 1 & 1 & 1 \\ 0 & 0 & 0 & 0 & 0 & 1 & 1 & 0 & 1 & 1 & 1 & 1 & 1 & 1 \\ 1 & 1 & 0 & 1 & 1 & 1 & 1 & 0 & 0 & 0 & 1 & 1 & 1 & 1 \\ 1 & 1 & 0 & 1 & 0 & 0 & 0 & 1 & 1 & 0 & 1 & 1 & 1 & 1 \\ 1 & 1 & 0 & 1 & 1 & 1 & 0 & 1 & 1 & 0 & 0 & 1 & 1 & 1 \\ 1 & 1 & 1 & 1 & 1 & 1 & 0 & 0 & 0 & 1 & 1 & 0 & 1 & 1 \\ 1 & 1 & 1 & 1 & 1 & 1 & 1 & 1 & 0 & 1 & 1 & 0 & 0 & 0 \\ 1 & 1 & 1 & 1 & 1 & 1 & 1 & 1 & 1 & 0 & 0 & 1 & 1 & 0 \\ 1 & 1 & 1 & 1 & 1 & 1 & 1 & 1 & 1 & 1 & 0 & 1 & 1 & 0 \\ 1 & 1 & 1 & 1 & 1 & 1 & 1 & 1 & 1 & 1 & 0 & 0 & 0 & 1 \end{bmatrix}$

Table 2. Visibility matrices for cross-sections of molecular electrostatic potential of DNA pyrimidine and purine bases. The values of level sets for MEP, indicated in parentheses, are in kcal/mol. The exterior visibility graph is used for the negative MEP contours

Molecule (a/kcal mol^{-1})	Visibility matrix	Molecule (a/kcal mol^{-1})	Visibility matrix
Cytosine (+4)	$\begin{bmatrix} 1 & 0 & 0 & 0 & 0 & 0 \\ 0 & 1 & 1 & 0 & 1 & 1 \\ 0 & 1 & 1 & 0 & 1 & 0 \\ 0 & 0 & 0 & 1 & 1 & 0 \\ 0 & 1 & 1 & 1 & 1 & 0 \\ 0 & 1 & 0 & 0 & 0 & 1 \end{bmatrix}$	Adenine (+4)	$\begin{bmatrix} 1 & 0 & 0 & 0 & 0 & 0 & 0 & 0 & 0 & 1 & 1 & 1 \\ 0 & 1 & 1 & 0 & 1 & 1 & 1 & 0 & 0 & 1 & 1 & 1 \\ 0 & 1 & 1 & 0 & 1 & 1 & 1 & 0 & 0 & 1 & 1 & 1 \\ 0 & 0 & 0 & 1 & 1 & 1 & 1 & 0 & 1 & 1 & 1 & 1 \\ 0 & 1 & 1 & 1 & 1 & 0 & 0 & 0 & 1 & 1 & 1 & 1 \\ 0 & 1 & 1 & 1 & 0 & 1 & 1 & 0 & 1 & 1 & 1 & 1 \\ 0 & 1 & 1 & 1 & 0 & 1 & 1 & 0 & 1 & 1 & 1 & 0 \\ 0 & 0 & 0 & 0 & 0 & 0 & 0 & 0 & 1 & 1 & 1 & 0 \\ 0 & 0 & 0 & 1 & 1 & 1 & 1 & 1 & 1 & 0 & 0 & 0 \\ 1 & 1 & 1 & 1 & 1 & 1 & 1 & 1 & 0 & 1 & 1 & 0 \\ 1 & 1 & 1 & 1 & 1 & 1 & 1 & 1 & 0 & 1 & 1 & 0 \\ 1 & 1 & 1 & 1 & 1 & 1 & 0 & 0 & 0 & 0 & 0 & 1 \end{bmatrix}$
Cytosine (−4)	$\begin{bmatrix} 1 & 1 & 1 & 1 \\ 1 & 1 & 0 & 0 \\ 1 & 0 & 1 & 1 \\ 1 & 0 & 1 & 1 \end{bmatrix}$	Adenine (−4)	$\begin{bmatrix} 1 & 1 & 1 & 1 & 1 & 1 \\ 1 & 1 & 1 & 1 & 1 & 1 \\ 1 & 1 & 1 & 1 & 1 & 1 \\ 1 & 1 & 1 & 1 & 1 & 1 \\ 1 & 1 & 1 & 1 & 1 & 1 \\ 1 & 1 & 1 & 1 & 1 & 1 \end{bmatrix}$
Uracil (+4)	$\begin{bmatrix} 1 & 0 & 0 & 0 & 1 & 1 & 1 & 1 \\ 0 & 1 & 1 & 0 & 1 & 1 & 1 & 1 \\ 0 & 1 & 1 & 0 & 0 & 1 & 1 & 1 \\ 0 & 0 & 0 & 1 & 1 & 0 & 1 & 0 \\ 1 & 1 & 0 & 1 & 1 & 0 & 0 & 0 \\ 1 & 1 & 1 & 0 & 0 & 1 & 1 & 0 \\ 1 & 1 & 1 & 1 & 0 & 1 & 1 & 0 \\ 1 & 1 & 1 & 0 & 0 & 0 & 0 & 1 \end{bmatrix}$	Guanine (+4)	$\begin{bmatrix} 1 & 0 & 0 & 0 & 0 & 0 \\ 0 & 1 & 1 & 0 & 1 & 1 \\ 0 & 1 & 1 & 0 & 0 & 0 \\ 0 & 0 & 0 & 1 & 1 & 0 \\ 0 & 1 & 0 & 1 & 1 & 0 \\ 0 & 1 & 0 & 0 & 0 & 1 \end{bmatrix}$
Uracil (−4)	$\begin{bmatrix} 1 & 1 & 1 & 1 \\ 1 & 1 & 1 & 1 \\ 1 & 1 & 1 & 1 \\ 1 & 1 & 1 & 1 \end{bmatrix}$	Guanine (−4)	$\begin{bmatrix} 1 & 1 & 0 & 0 & 0 \\ 1 & 1 & 0 & 0 & 0 \\ 0 & 0 & 1 & 1 & 0 \\ 0 & 0 & 1 & 1 & 0 \\ 0 & 0 & 0 & 0 & 0 \end{bmatrix}$

the cross-section is formed by at least two closed curves, one of which is convex (no inflexion points present).

The results for the level set of MEP corresponding to +4 kcal/mol show the occurrence of single closed curve. For all the four compounds we have followed the same convention to number the inflexion points (interior visibility graphs are

used here). Furthermore, the vertex V_1 was chosen to be the one closest to the zero electrostatic potential contour line. This consistency in the labeling of the points allows one to make meaningful shape comparisons. Observe, for example, that the first 4×4 block of the visibility matrices is the same for all the four compounds. This similarity extends to the first 5×5 block in the cas of adenine and cytosine. These coincidences suggest that, despite the presence of different atoms in the molecules, some general shape features of the cross-section remain much the same for these compounds.

The above results may help the development of a prospective, automated analysis of molecular similarities using the discrete characterization of molecular surface cross-sections. Furthermore, it can be useful in developing a rigorous criterion to assess the shape complementarity of two sections of different molecular surfaces. The problem of complementarity between different molecular surfaces is of importance when describing drug-receptor interactions, or enzyme-substrate complexes, in general. In principle, two complementary sections of molecular surfaces should exhibit *common blocks of their visibility matrices*, when the exterior representation is adopted for viewing one of the molecules, and the interior representation for viewing the second one.

5. Further comments

In the preceding sections we have discussed and analyzed cross-sections of molecular surfaces that are differentiable everywhere. In this last section we make some comments with respect to possible generalizations of this approach.

Analyzing cross-sections of hard-sphere surfaces (the so-called van-der-Waals-like surfaces) poses the problem that the curves will not be, in general, differentiable everywhere. These surfaces are the envelope surfaces determined by the interpenetration of spheres. As a consequence, at some points no derivative exists, and the value of the second derivative in the local system, when it exists, will be always negative (convex sections). However, the method can be extended naturally to treat these systems, by means of a simple modification: *the vertices of the graph are formed by all the points of the cross-section where the curve is not differentiable.* The visibility among vertices, $\mathrm{vis}((\boldsymbol{V}_i, \boldsymbol{V}_j))$, is defined as in the second section. The graph will be indicated by $g'_n(a, K, P)$ to distinguish it from the previous types. Notice that each vertex in $g'_n(a, K, P)$ can be viewed as a degenerate case where two vertices, limiting a concave section in a differentiable planar curve, approach one another and become coincident.

The graph constructed according to the above rules possesses some properties differing from those of the original graph $g_n(a, K, P)$. The occurrence of only convex neighborhoods (for the points where the cross-section is differentiable) implies that every vertex can always see its two closest neighbor vertices (at least when the cross-section is a single curve). That is, Eq. (16) will not hold in general for $\boldsymbol{v}(g'_n(a, K, P))$.

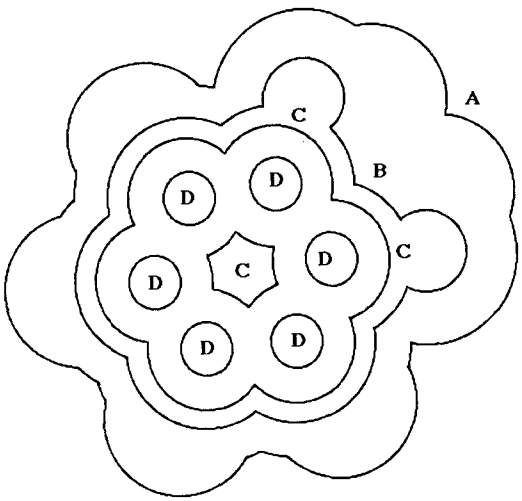

Figure 8. Schematic representation of cross-sections of the van der Waals surface of 1,2-dihydroxybenzene (catechol) in a planar configuration. *A*: plane $z = 0$ Å; *B*: plane $z = 1.25$ Å; *C*: plane $z = 1.50$ Å; *D*: plane $z = 1.70$ Å

Figure 8 provides an illustrative example of VDWS cross-sections. The example considered is a planar configuration of the molecule of 1,2-dihydroxybenzene (catechol). This configuration corresponds to a case with the two hydroxylic hydrogen atoms closest to each other (symmetry C_{2v}); this is one of the local minima of the energy hypersurface. The molecule is built from atoms of different "sizes" and it has some interesting shape features. In our case the geometry was computed at the *ab initio* STO-3G level with the program GAUSSIAN 86 of Pople and co-workers. In order to construct the VDWS, the van der Waals atomic radii were taken from Ref. [57]. Some of the representative cross-sections appear in Fig. 8. The molecular plane coincides with the plane $z = 0$ (i.e., $P = P(0, 0, 1, 0)$); accordingly, the different cross-sections show an elevation map of the VDWS. The first contour line ($z = 0$) reveal the presence of all the atoms in the molecule. The second curve ($z = 1.20$ Å) has been chosen so that the hydrogen atoms (with a van der Waals radius of 1.17 Å) are not seen. For the third and fourth contours ($z = 1.50$ and $z = 1.70$ Å, respectively) all the shape features are associated with the carbon atoms. Table 3 contains a concise representation of all the results obtained by displaying the visibility matrices of the corresponding graphs. Notice that the off-diagonal elements closest to the diagonal are all 1 for the first three matrices, as commented above. On the other hand, the visibility matrix for the $z = 1.70$ contour has only zero elements, due to the fact that the cross-section is composed by 6 disjoint, closed convex curves.

This characterization of hard-sphere surfaces is a straightforward extension of the characterization for smooth, differentiable molecular surfaces. The description is simple and allows one to represent some essential shape features of the surface in a numerical nonvisual fashion. According to our proposal, one can obtain a simple, numerical representation of a VDWS by calculating the visibility matrices of a number of its cross-sections.

Table 3. Visibility matrices for several cross-sections of a planar configuration (local minimum) of 1,2-dihydroxybenzene (catechol)

Plane considered	Visibility matrix
$P(0, 0, 1, 0)$	$\begin{bmatrix} 1 & 1 & 1 & 0 & 1 & 1 & 1 & 1 & 1 & 1 & 1 & 1 & 1 & 0 & 1 & 1 \\ 1 & 1 & 1 & 0 & 1 & 1 & 1 & 1 & 1 & 1 & 1 & 1 & 1 & 1 & 1 & 1 \\ 1 & 1 & 1 & 1 & 1 & 1 & 1 & 1 & 1 & 1 & 1 & 1 & 1 & 1 & 1 & 1 \\ 0 & 0 & 1 & 1 & 1 & 1 & 1 & 1 & 1 & 1 & 1 & 1 & 1 & 1 & 1 & 1 \\ 1 & 1 & 1 & 1 & 1 & 1 & 0 & 1 & 1 & 1 & 1 & 1 & 1 & 1 & 1 & 1 \\ 1 & 1 & 1 & 1 & 1 & 1 & 1 & 1 & 1 & 1 & 1 & 1 & 1 & 1 & 1 & 1 \\ 1 & 1 & 1 & 1 & 0 & 1 & 1 & 1 & 1 & 1 & 1 & 1 & 1 & 1 & 1 & 1 \\ 1 & 1 & 1 & 1 & 1 & 1 & 1 & 1 & 1 & 0 & 1 & 1 & 1 & 1 & 1 & 1 \\ 1 & 1 & 1 & 1 & 1 & 1 & 1 & 1 & 1 & 1 & 1 & 1 & 1 & 1 & 1 & 1 \\ 1 & 1 & 1 & 1 & 1 & 1 & 1 & 0 & 1 & 1 & 1 & 1 & 1 & 1 & 1 & 1 \\ 1 & 1 & 1 & 1 & 1 & 1 & 1 & 1 & 1 & 1 & 1 & 1 & 0 & 1 & 1 & 1 \\ 1 & 1 & 1 & 1 & 1 & 1 & 1 & 1 & 1 & 1 & 1 & 1 & 1 & 1 & 1 & 1 \\ 1 & 1 & 1 & 1 & 1 & 1 & 1 & 1 & 1 & 1 & 0 & 1 & 1 & 1 & 1 & 1 \\ 0 & 1 & 1 & 1 & 1 & 1 & 1 & 1 & 1 & 1 & 1 & 1 & 1 & 1 & 1 & 0 \\ 1 & 1 & 1 & 1 & 1 & 1 & 1 & 1 & 1 & 1 & 1 & 1 & 1 & 1 & 1 & 1 \\ 1 & 1 & 1 & 1 & 1 & 1 & 1 & 1 & 1 & 1 & 1 & 1 & 1 & 0 & 1 & 1 \end{bmatrix}$
$P(0, 0, 1, 1.25)$	$\begin{bmatrix} 1 & 1 & 1 & 1 & 1 & 1 & 1 & 1 & 1 & 1 \\ 1 & 1 & 1 & 1 & 1 & 1 & 1 & 1 & 1 & 0 \\ 1 & 1 & 1 & 1 & 1 & 1 & 1 & 1 & 1 & 1 \\ 1 & 1 & 1 & 1 & 1 & 1 & 1 & 1 & 1 & 1 \\ 1 & 1 & 1 & 1 & 1 & 1 & 1 & 1 & 1 & 1 \\ 1 & 1 & 1 & 1 & 1 & 1 & 1 & 1 & 1 & 1 \\ 1 & 1 & 1 & 1 & 1 & 1 & 1 & 1 & 1 & 1 \\ 1 & 1 & 1 & 1 & 1 & 1 & 1 & 1 & 1 & 1 \\ 1 & 1 & 1 & 1 & 1 & 1 & 1 & 1 & 1 & 1 \\ 1 & 0 & 1 & 1 & 1 & 1 & 1 & 1 & 1 & 1 \end{bmatrix}$
$P(0, 0, 1, 1.50)$	$\begin{bmatrix} 1 & 1 & 0 & 0 & 0 & 1 & 1 & 1 & 0 & 0 & 0 & 1 \\ 1 & 1 & 1 & 0 & 0 & 0 & 1 & 1 & 1 & 0 & 0 & 0 \\ 0 & 1 & 1 & 1 & 0 & 0 & 0 & 1 & 1 & 1 & 0 & 0 \\ 0 & 0 & 1 & 1 & 1 & 0 & 0 & 0 & 1 & 1 & 1 & 0 \\ 0 & 0 & 0 & 1 & 1 & 1 & 0 & 0 & 0 & 1 & 1 & 1 \\ 1 & 0 & 0 & 0 & 1 & 1 & 1 & 0 & 0 & 0 & 1 & 1 \\ 1 & 1 & 0 & 0 & 0 & 1 & 1 & 1 & 0 & 0 & 0 & 1 \\ 1 & 1 & 1 & 0 & 0 & 0 & 1 & 1 & 1 & 0 & 0 & 0 \\ 0 & 1 & 1 & 1 & 0 & 0 & 0 & 1 & 1 & 1 & 0 & 0 \\ 0 & 0 & 1 & 1 & 1 & 0 & 0 & 0 & 1 & 1 & 1 & 0 \\ 0 & 0 & 0 & 1 & 1 & 1 & 0 & 0 & 0 & 1 & 1 & 1 \\ 1 & 0 & 0 & 0 & 1 & 1 & 1 & 0 & 0 & 0 & 1 & 1 \end{bmatrix}$
$P(0, 0, 1, 1.70)$	$\begin{bmatrix} 0 & 0 & 0 & 0 & 0 & 0 \\ 0 & 0 & 0 & 0 & 0 & 0 \\ 0 & 0 & 0 & 0 & 0 & 0 \\ 0 & 0 & 0 & 0 & 0 & 0 \\ 0 & 0 & 0 & 0 & 0 & 0 \\ 0 & 0 & 0 & 0 & 0 & 0 \end{bmatrix}$

Acknowledgment. One of us (G.A.A.) would like to thank Drs. M. Dupuis and H. O. Villar for the use of their computer facilities to study contours of total electronic density, and for their warm hospitality while visiting the Department of Scientific Computations, IBM Corporation, Kingston, New York, where part of this work was performed. We would also like to thank Dr. F. Sanz (Barcelona) for sending us a copy of Ref. [55] prior to publication. This work was supported by a research grant from the Natural Sciences and Engineering Research Council (NSERC) of Canada.

References

1. Richards WG (1983) Quantum pharmacology. Butterworths, London
2. Franke R (1984) Theoretical drug design methods. Pharmacochemistry library, vol 7. Elsevier, Amsterdam
3. Dearden JC (1983) Quantitative approaches to drug design. Pharmacochemistry library, vol 6. Elsevier, Amsterdam
4. Bonaccorsi R, Scrocco E, Tomasi J (1974). In: Bergman ED, Pullman B (eds) Chemical and biochemical reactivity. Reidel, Dordrecht
5. Scrocco E, Tomasi J (1973) Top Curr Chem 42:95; Scrocco E, Tomasi J (1978) Adv Quantum Chem 11:115
6. Tomasi J (1979) In: Daudel R, Pullman A, Salem L, Veillard A (eds) Quantum theory of chemical reactions, vol 1. Reidel, Dordrecht
7. Politzer P, Truhlar DG (1981) Chemical applications of atomic and molecular electrostatic potentials. Plenum Press, New York
8. Weinstein H, Osman R, Topiol S, Venanzi CA (1983) p 81 in [3]
9. Rein R, Rabinowitz JR, Swissler TJ (1972) J Theor Biol 34:215
10. Reggio PH, Weinstein H, Osman R, Topiol S (1981) Int J Quantum Chem, Quantum Biol Symp 8:373
11. Thornber CW (1979) Chem Soc Rev 8:563
12. Warshel A (1981) Acc Chem Res 14:284
13. Náray-Szabó G (1980) QCPE 13:396
14. Náray-Szabó G, Grofcsik A, Kósa K, Kubinyi M, Martin A (1981) J Comput Chem 2:58
15. Ángyán J, Náray-Szabó G (1983) J Theor Biol 103:777
16. Gabányi Z, Surján P, Náray-Szabó G (1982) Eur J Med Chem 17:307
17. Louie AH, Somorjai RL (1982) J Theor Biol 98:189
18. Hout RF, Hehre WJ (1983) J Am Chem Soc 105:3728
19. Francl MM, Hout RF, Hehre WJ (1984) J Am Chem Soc 106:563
20. Purvis GD, Culberson C (1986) Int J Quantum Chem, Quantum Biol Symp 13:261
21. Langridge R, Ferrin TE, Kuntz ID, Connolly ML (1981) Science 211:661
22. Pearl LH, Honegger A (1983) J Mol Graph 1:9
23. Connolly ML (1983) Science 221:709
24. Kahn SD, Pau CF, Overman LE, Hehre WJ (1986) J Am Chem Soc 108:7381
25. Carbó R, Arnau M (1981) In: De las Heras FG, Vega S (eds) Medicinal chemistry advances. Pergamon Press, Oxford
26. Martín M, Sanz F, Campillo M, Pardo L, Pérez J, Turmo J, Agullo JM (1983) Int J Quantum Chem 23:1643
27. Bowen-Jenkins PE, Cooper DL, Richards WG (1985) J Phys Chem 89:2195
28. Richard AM, Rabinowitz JR (1987) Int J Quantum Chem 31:309
29. Carbó R, Domingo Ll (1987) Int J Quantum Chem 32:517
30. Lee B, Richards FM (1971) J Mol Biol 55:379
31. Richards FM (1977) Annu Rev Biophys Bioeng 6:151
32. Greer J, Bush BL (1978) Proc Natl Acad Sci USA 75:303
23. Pfeifer P, Welz U, Wippermann H (1985) Chem Phys Lett 113:535
34. Lewis M, Rees DC (1985) Science 230:1165
35. Åqvist J, Tapia O (1987) J Mol Graph 5:30
36. Mezey PG (1986) Int J Quantum Chem, Quantum Biol Symp 12:113

37. Mezey PG (1987) J Comput Chem 8:462
38. Mezey PG (1987) Int J Quantum Chem, Quantum Biol Symp 14:127
39. Arteca GA, Mezey PG (1987) Int J Quantum Chem, Quantum Biol Symp 14:133
40. Arteca GA, Mezey PG (1988) Int J Quantum Chem, Quantum Biol Symp in press
41. Arteca GA, Mezey PG (1988) J Comput Chem 9:554
42. Arteca GA, Mezey PG (1988) THEOCHEM 43:11
43. Arteca GA, Mezey PG: J Math Chem, to be published
44. Arteca GA, Jammal VB, Mezey PG (1988) J Comput Chem 9:608
45. Arteca GA, Jammal VB, Mezey PG, Yadav JS, Hermsmeier MA, Gund TM (1988) J Mol Graph 6:45
46. Pipek J, Mezey PG (1988) Int J Quantum Chem, Quantum Chem Symp, in press
47. Harary F (1969) Graph theory. Addison-Wesley, Reading, Mass
48. Mezey PG (1988) J Math Chem, in press
49. Arteca GA, Mezey PG (1988) Int J Quantum Chem, in press
50. Harary F, Mezey PG (1988) J Math Chem, in press
51. Mezey PG (1987) Potential energy hypersurfaces. Elsevier, Amsterdam
52. Mezey PG (1980) Theor Chim Acta 54:95
53. Dupuis M, Watts JD, Villar HO, Hurst GJB (1988) HONDO: Version 7.9, IBM Corporation, Kingston, New York
54 Arteca GA, Mezey PG, in preparation
55. Sanz F, Manaut F, José J, Segura J, Carbó M, De la Torre R (1988) THEOCHEM 47:171
56. Eisenstein M (1988) Int J Quantum Chem 33:127
57. Gavezzotti A (1983) J Am Chem Soc 105:5220